Journal of Physics: Conference Series **579** (2015) 012010 doi:10.1088/1742-6596/579/1/012010

On the performance of a high head Francis turbine at design and off-design conditions

B Aakti, O Amstutz, E Casartelli, G Romanelli, L Mangani

Lucerne University of Applied Sciences and Arts Engineering & Architecture, Horw Switzerland

E-mail: ernesto.casartelli@hslu.ch

Abstract. In the present paper, fully 360 degrees transient and steady-state simulations of a Francis turbine were performed at three operating conditions , namely at part load (PL), best efficiency point (BEP), and high load (HL), using different numerical approaches for the pressure-velocity coupling. The simulation domain includes the spiral casing with stay and guide vanes, the runner and the draft tube. The main target of the investigations is the numerical prediction of the overall performance of the high head Francis turbine model as well as local and integral quantities of the complete machine in different operating conditions. All results were compared with experimental data published by the workshop organization. All CFD simulations were performed at model scale with a new in-house, 3D, unstructured, object-oriented finite volume code within the framework of the open source OpenFOAM library. The novel fully coupled pressure-based solver is designed to solve the incompressible RANS-Equations and is capable of handling multiple references of frame (MRF). The obtained results show that the overall performance is well captured by the simulations. Regarding the local flow distributions within the inlet section of the draft-tube, the axial velocity is better estimated than the circumferential component.

1. Introduction

The scope of the first Francis-99 workshop is the assessment of advanced numerical tools for the prediction of steady-state operating points in a Francis turbine for design and off-design conditions [1]. The continuous evolution of the numerical techniques and the computer power has lead in the last decade to a large tool-spectrum for turbomachinery investigations. The driver for this trend was mainly the only partly-satisfactory results obtained, especially at off-design conditions. The main reasons for the discrepancies were located firstly in the turbulence models, with the development of more advanced models capable to improve the drawbacks of classical models like $k-\epsilon$ and capture additional flow physics, like curvature correction for the SST model or the v2F model and secondly in the thought inability of steady-state methods to properly predict the inherently unsteady effects present in turbomachines [2], [3].

In the present paper a comparison of steady and unsteady computations for the 360 degrees model are presented within the framework of OpenFOAM, performing the simulations with two different computational technologies, the segregated and the coupled one. For steady-state computations, the coupled technology has clear and well known advantages [4], leading to a speed-up of factors, typically 3 to 10, depending on the mesh size.

For transient cases, with a typical time step corresponding to mesh motion of 1 degree or less,

the CFL can be considerably larger than 1. In these cases the use of a fully implicit approach like in the coupled solver is beneficial. In these cases a speed up of additional 50% is obtained, thus underlining the power of a coupled approach also for unsteady cases.

2. CFD - solver technology

2.1. Governing equation

The Unsteady Reynolds Averaged Navier-Stokes (URANS) equations governing the dynamics of an incompressible, viscous flow can be written within an Arbitrary Lagrangian Eulerian (ALE) framework in differential form as follows:

$$\nabla \cdot \mathbf{u} = 0 \tag{1}$$

$$\frac{\partial \mathbf{u}}{\partial t} + \nabla \cdot (\mathbf{u}_\mathrm{r}\mathbf{u}) = -\frac{1}{\rho}\nabla p + \nabla \cdot (\nu_\mathrm{eff}\nabla \mathbf{u}) \tag{2}$$

where $\mathbf{u}$ is the absolute velocity, p the pressure and ρ the density of the fluid. The convecting flux is written in terms of the relative velocity $\mathbf{u}_\mathrm{r} = \mathbf{u} - \mathbf{u}_\mathrm{ALE}$, where $\mathbf{u}_\mathrm{ALE}$ is the velocity associated to the dynamic motion (either rigid and/or deformable) of the physical domain $V = V(t)$ and it is evaluated enforcing the so-called Geometric Conservation Law (GCL). For instance, for a purely rigid rotation with constant angular velocity $\mathbf{\Omega}$, it corresponds to $\mathbf{u}_\mathrm{ALE} = \mathbf{\Omega} \times \mathbf{r}$. Finally the effective kinematic viscosity is the sum of the laminar and turbulent kinematic viscosities ($\nu_\mathrm{eff} = \nu + \nu_\mathrm{t}$).

2.2. Numerical discretization

Speed and robustness are among the most important requirements for any software that has to be used for the time-accurate numerical analysis of complex highly unsteady phenomena. When programming a CFD code the best way of combining both requirements is to couple the governing equations implicitly, since resolving efficiently the pressure-velocity coupling is essential for the performance of any CFD code. However up until today the SIMPLE family of algorithms [5], which couples the governing equations only by means of sub-looping, solving sequentially each governing equation, still remains the predominant methodology used in the CFD community. Therein a segregated approach in resolving the pressure velocity coupling is followed. Compared to block coupled implicit algorithms, segregated algorithms lack scalability with mesh size, robustness and calculation speed, which is inherent due in part to the under-relaxation needed to stabilize the algorithm. This is even more critical for unsteady simulations, as a set of inner non-linear iterations must be accounted for in order to drive the solver to the desired accuracy level in time.

In order to overcome these shortcomings Mangani et al. [4] developed a block coupled incompressible solver using the open-source CFD library OpenFOAM® as programming platform. Therein the algebraic equations resulting from the Navier-Stokes equations are solved simultaneously with the following system of equations, where 'C' are the cell values while 'NB' the neighbor contributions:

$$\begin{bmatrix} a_C^{uu} & a_C^{uv} & a_C^{uw} & a_C^{up} \\ a_C^{vu} & a_C^{vv} & a_C^{vw} & a_C^{vp} \\ a_C^{wu} & a_C^{wv} & a_C^{ww} & a_C^{wp} \\ a_C^{pu} & a_C^{pv} & a_C^{pw} & a_C^{pp} \end{bmatrix} \cdot \begin{bmatrix} u_C \\ v_C \\ w_C \\ p_C \end{bmatrix} + \sum_{NB} \begin{bmatrix} a_{NB}^{uu} & a_{NB}^{uv} & a_{NB}^{uw} & a_{NB}^{up} \\ a_{NB}^{vu} & a_{NB}^{vv} & a_{NB}^{vw} & a_{NB}^{vp} \\ a_{NB}^{wu} & a_{NB}^{wv} & a_{NB}^{ww} & a_{NB}^{wp} \\ a_{NB}^{pu} & a_{NB}^{pv} & a_{NB}^{pw} & a_{NB}^{pp} \end{bmatrix} \cdot \begin{bmatrix} u_{NB} \\ v_{NB} \\ w_{NB} \\ p_{NB} \end{bmatrix} = \begin{bmatrix} b_C^u \\ b_C^v \\ b_C^w \\ b_C^p \end{bmatrix} \tag{3}$$

To further enhance computational performance an algebraic multi-grid solver has been implemented and used for the solution of the block-coupled system of linearized equations presented above.

While segregated algorithms operate using many under-relaxed sub-loops to account for inter-equation coupling, the inter-variable coupling is much stronger and less sub-loops are needed. Moreover no under-relaxation is needed. The solution of such a discretized system of equations therefore results to be numerically much more stable than that of segregated algorithms and also turns out to be significantly faster in terms of calculation time, which has been demonstrated by Mangani et al. [4]. The solver described in [4] has been used for the unsteady simulations carried out in this work and compared with the results of a reference commercial solver. More details regarding the modeling choices, the numerical set-up and the initial and boundary conditions are provided below.

2.3. Turbulence modeling

All the simulations were performed using a $k-\omega$ SST turbulence model which requires the numerical solution of two scalar equations for the turbulent conservation variables (not coupled) in addition to momentum and continuity equations. Although two-equation turbulence models are known to have shortcomings at off-design conditions, even flow instabilities can be investigated, as shown in [6, 7], where they are captured and fairly agree with experimental data. The choice of the SST turbulence model is based on the fact that it is a sort of industrial standard and widely used [8, 9, 10, 11]. Moreover, the automatic wall functions are applicable using the SST.

2.4. Domain discretization

The simulation domain ranges from the spiral case inlet, the stay vanes, the guide vanes and runner to the draft tube as shown in figure 1. For the three operating points, the guide vane opening angles are defined as 9.84, 3.91 and 12.44 degrees at BEP, PL and HL, respectively. Further geometrical details of the model are given in [12], [13].

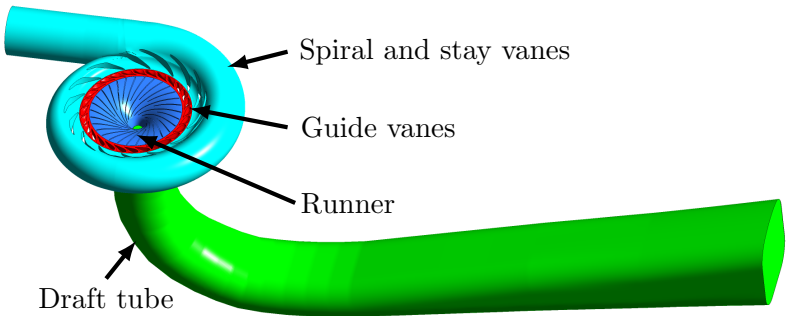

Figure 1: The four simulation domains of the Francis-99 turbine.

The global structured mesh encompassed approximately 16.5 million hexahedral distributed in 4 cell zones (spiral/stay-vanes, guide-vanes, rotor and draft tube). The runner domain has been discretized appling ANSYS ICEM v14.5, where as the other domains have been created with Pointwise v17.2R1. Rotating and stationary domains were matched using transient rotor stator Arbitrary Mesh Interfaces (AMI). The geometry of the mesh is taken by the provided data from the Francis-99 workshop, but the mesh is recreated. No further mesh study was performed. The quality of the mesh corresponds the usual industrial standard. Table 1 summarizes the detailed mesh quality of the individual computation domains.

Table 1: Mesh Quality.

HSLU-Mesh	Element size	Y^+ (BEP)	Angle	Volume change	Aspect ratio
Global	16'580'697	21.8	2.8	97	1421
Spiral & stay vanes	5'331'788	19.1	3.5	50	1421
Guide vanes BEP	3'780'280	26.9	19.5	56	58
Guide vanes PL	3'780'280	19.4	17.2	97	153
Guide vanes HL	3'780'280	23.6	16.0	55	73
Runner	5'983'950	15.7	2.8	21	305
Draft tube	1'484'679	21.8	51.8	8	250

The rotor side spaces were neglected so that disc friction as well as leakage flow were not directly available in the simulations. In order to estimate the overall effect of the neglected leakage within the rotor side spaces, an in-house tool [14] has been used to determine the friction torque in the leakage gap. The in-house tool uses interpolation equations which, from an extensive dataset based on detailed parameter studies of rotor side spaces, extract the corresponding correlation values [15]. The calculation is limited to the leakage gap on the shroud side of the runner because on the hub side of the runner there are no pressure relief-holes and therefore the influence is considered as not relevant. At BEP conditions, the friction torque within the leakage gap is 9.53 Nm which corresponds to 1.8% of the measured blade torque. At HL and PL, the friction torque is 1.5% and 8.0%, respectively. These values are used to correct the measured efficiency, thus leading to higher values, which are then in good agreement with the computed efficiency.

2.5. Numerical schemes

All the simulations were performed with fully second order upwind space discretization operators. The second order upwind operator uses a special gradient extrapolation[4]. Moreover ad-hoc switching to spatial first order was not necessary at the beginning of the simulations for stability issues as instead usually required by the standard simpleFoam solver [16]. A fully second-order time discretization is achieved by means of inner non-linear iterations (for the present simulations 4-6 sub-iterations were sufficient to achieve a drop of 5 orders of magnitude of the inner residuals), using a time step which is corresponding to a resolution of the rotor motion of 0.25 deg. The small timestep is chosen according to the large number of main- and splitterblades. For example a resolution of the rotor motion of 1 deg. would lead to only 12 steps per blade. Starting from the steady-state solution, the time step has been decreased stepwise (waiting each time until a for periodic oscillation was reached) from a rotor motion corresponding to 5 deg, 1 deg, 0.5 deg to finally 0.25 deg. The convergence of the frozen rotor calculations is at least 10^{-4} RMS respective 10^{-2} maximum residuals. The convergence of the transient simulation is for RMS 10^{-5} and for the maximum residuals 10^{-3}.

2.6. Initial and boundary conditions

All unsteady simulations have been initialized with a steady-state Multiple Reference Frames (MRF) solution. At the inlet of the computational domain the velocity $\mathbf{u}_{\text{inlet}}$, the turbulent kinetic energy (k), and the turbulent frequency (ω) are imposed as a fixed value. The turbulence variables k, ϵ and ω are initialized as $k = 3/2(I|\mathbf{u}_{\text{inlet}}|)^2$, $\epsilon = C_\mu^{0.75} k^{1.5}/\ell$ and $\omega = \epsilon/k/C_\mu$ respectively, where I is the prescribed turbulence intensity of 0.05 respectively 5%, $C_\mu = 0.09$ is a constant turbulence model parameter and ℓ is the turbulent mixing length scale. At the outlet of the computational domain, an average static pressure of $p_{\text{outlet}} = 0$ Pa is used. The walls in the domains are non-rotating, except for the runner (hub, blade and shroud). At the walls, a

no-slip condition is imposed. The runner domain rotates around the negative z-axis. The only difference in the numerical setup between the coupled and the segregated is the discretization of the convection term. Nevertheless, both are second order [17].

2.7. Comparison of computational time

In the frozen rotor case (steady-state), the coupled solver is approximately 4 to 5 times faster than the segregated solver, depending on the operating point. For transient simulations, where small time steps are used, the segregated solver is usually a more adequate tool to use. Nevertheless the coupled solver is still faster by a factor of 1.5 than the segregated one, mainly because of the big mesh size.

3. Results

3.1. Integral values

In order to predict the performance of the Francis turbine, time accurate transient simulations as well as steady-state (frozen rotor) simulations were carried out. Figure 2 summarizes the results of the transient as well as the steady-state results. In each sub-figure, a comparison of the Commercial Code (CC), OpenFOAM coupled solver (OF coupled) , OpenFOAM segregated solver (OF segregated) and the measurements provided by the Francis-99 workshop [1] is given.

In all simulations (see figure 2a), the efficiency has been overestimated. The main reason for this overestimation is because the rotor side spaces are neglected in the simulation and therefore all the associated losses are not considered. Assuming that the efficiency difference is proportional to the friction torque, the measured efficiency has been corrected by the estimated friction torque (Exp. corr.). For the sake of clarity, the measured efficiency is corrected and not the results of the simulations. The effect of the leakage flow at the rotor side spaces is not used in the correction of the efficiency.

At BEP operating conditions, all transient simulations predict the corrected measured efficiency well. At off-design conditions, the segregated OpenFOAM solver estimates the efficiency of the turbine closest to the measurements. At PL, the coupled OpenFOAM solver is furthest away from the measurements and at HL, the reference commercial solver.

Figure 2b gives an overview of the performance of the steady-state simulations using the frozen rotor approach. Overall, the steady-state frozen rotor results matches the measurements well. This could be an impact of the evenly distributed flow in the guide vane channels. At all operating conditions, the OpenFOAM segregated solver estimates the efficiencies closest to the measurements followed by the coupled OpenFOAM solver. While at BEP operating conditions all CFD codes perform approximately the same, at off-design conditions, the presented OpenFOAM solvers predict the integral values of the turbine closer to the experiments than the reference commercial solver. The difference in the results between the segregated and the coupled solver should be due to the different second order convection term scheme.

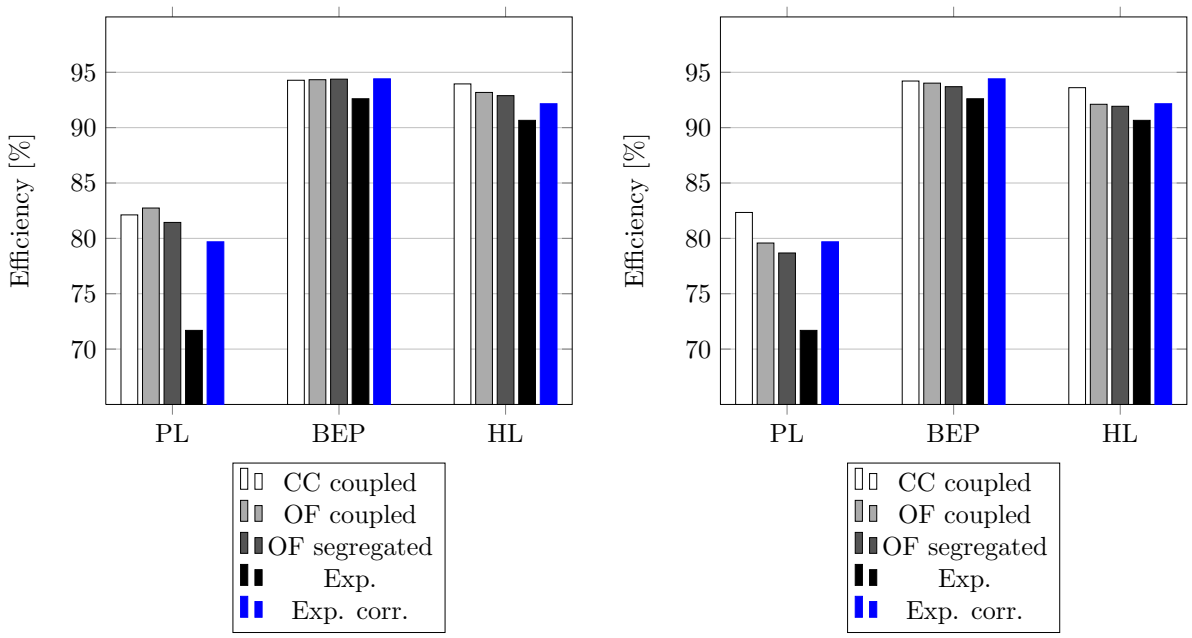

(a) Efficiency transient (b) Efficiency frozen rotor

Figure 2: Efficiency in all operating points.

According to figure 3, the vortex rope in all operating conditions but especially in part load is surprisingly straight. The straight vortex rope could be a explanation for the good frozen rotor results compared to the measurements as well as the transient simulation results.

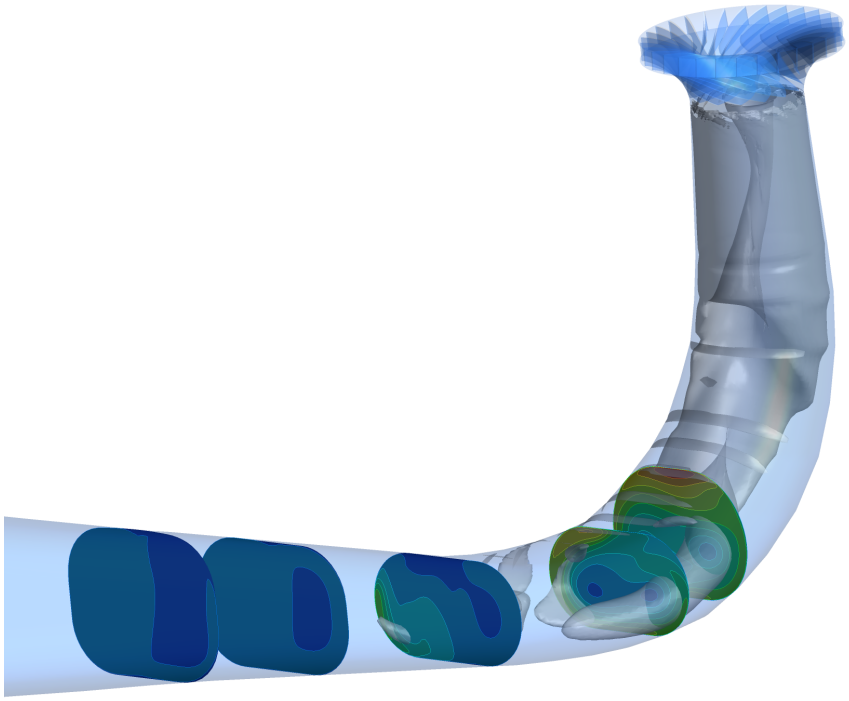

Figure 3: Vortex rope in PL operating point. On the contour planes is the velocity plotted and the vortex rope is displayed with the swirling strength.

3.2. Local data

The Francis-99 workshop provided pressure measurement data at different probe point locations. There are two points within the simulation domain, as shown in figure 4.

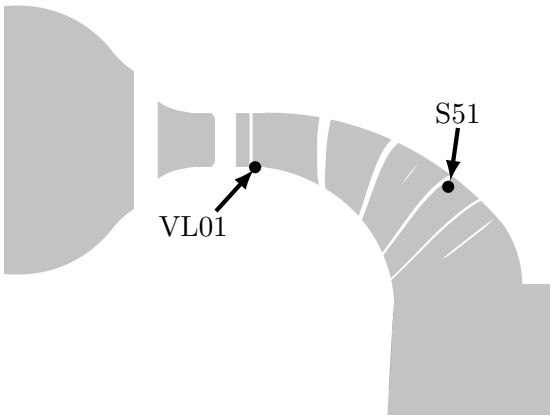

Figure 4: Probe point locations.

In order to visualize the dominant frequencies, fast Fourier transformations (FFT) have been performed. The y-axis represents the normalized pressure amplitude. The measurement provided by the workshop showed broad band noise after the FFT, therefore only the CFD data has been analyzed. The frequency of the main and splitter blades at the given operating conditions are 167.7 Hz at BEP, 184.8 Hz at HL and 203.1 Hz at PL. As shown in figures 5 and 6, the blade frequency is dominant. All three CFD codes are showing the same characteristic frequencies.

In S51 is the amplitude in the part load condition dominant. Due to the fact that at this operating point the flow is largely separated at the entrance of the runner, i.e. just before the measuring point.

At the probe point VL01, which is located very close or even between the guide vanes depending on the operating point, the frequency of the main blades (84 Hz / 92 Hz / 102 Hz) is clearly visible. Due to this position the amplitude of the pressure signal is relatively low.

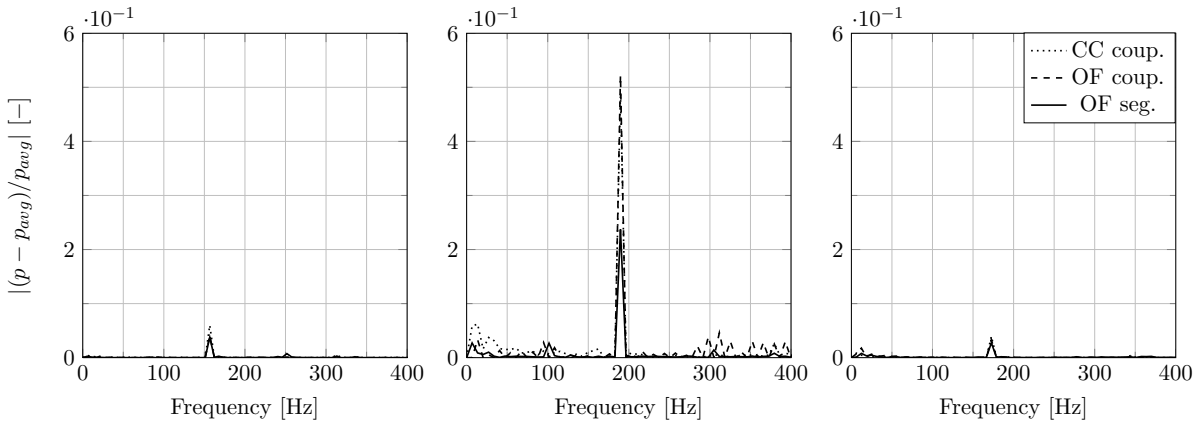

(a) BEP (b) PL (c) HL

Figure 5: FFT signal of S51.

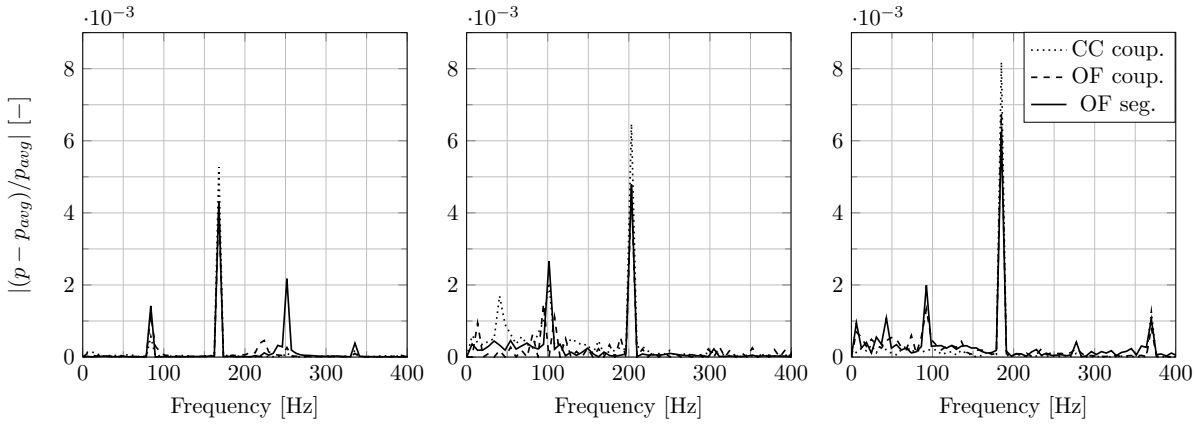

(a) BEP (b) PL (c) HL

Figure 6: FFT signal of VL01.

3.3. LDA Measurements

In the following, the mean axial and tangential velocity profiles along the radius at two measuring sections (LDA cut planes), as described in figure 7, are compared. All presented velocities have been normalized using the mean axial velocity at the draft tube inlet, which is upstream of the top plane. In order to ensure a good comparability of the CFD and the Laser Doppler Anemometry (LDA) results, the velocities predicted by CFD have been evaluated exactly at the same position as the LDA measurements. The results of the transient simulation have been averaged over one runner passage.

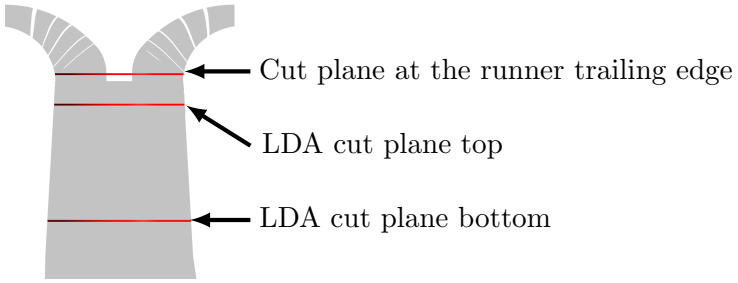

Figure 7: Position of the evaluation planes.

The resulting velocity profiles of the transient simulations are shown in figures 8 to 14. The discrepance between measurements and the different frozen rotor results are similar to the transient ones. Therefore these results are not presented. In general the axial velocity distribution is captured better than the tangential component. The reference commercial solver usually predicted the axial velocity better compared to the OpenFOAM solvers. On the other hand the tangential velocity has been highly overestimated by all three solvers. The OpenFOAM coupled solver is at BEP conditions and at HL condition the furthest away form the measurement, whereas the reference commercial solver is closest to the experimental results. A discussion of the discrepancy between the numerically predicted tangential velocities and the experimental results is given in section 3.4. At PL operating conditions all simulation-results are similar. The difference to the measurement is small compared to that observed at BEP and HL.

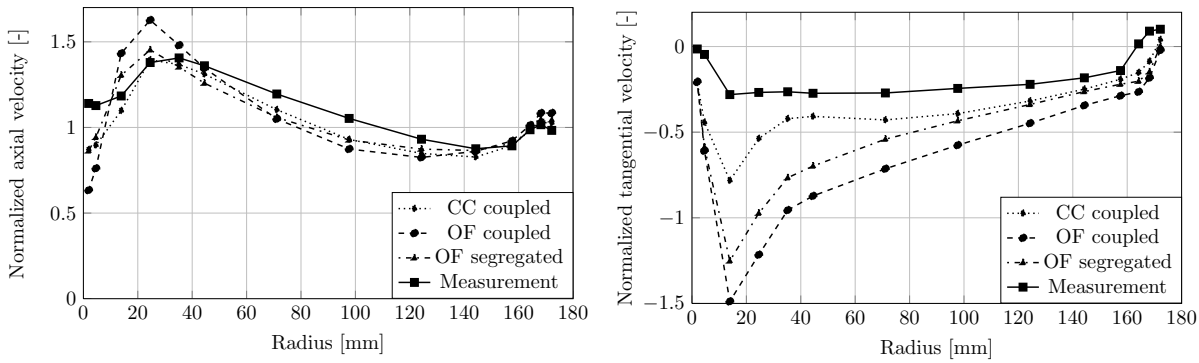

(a) Axial velocity (b) Tangential velocity

Figure 8: Normalized axial and tangential velocity at top slice in transient BEP operation.

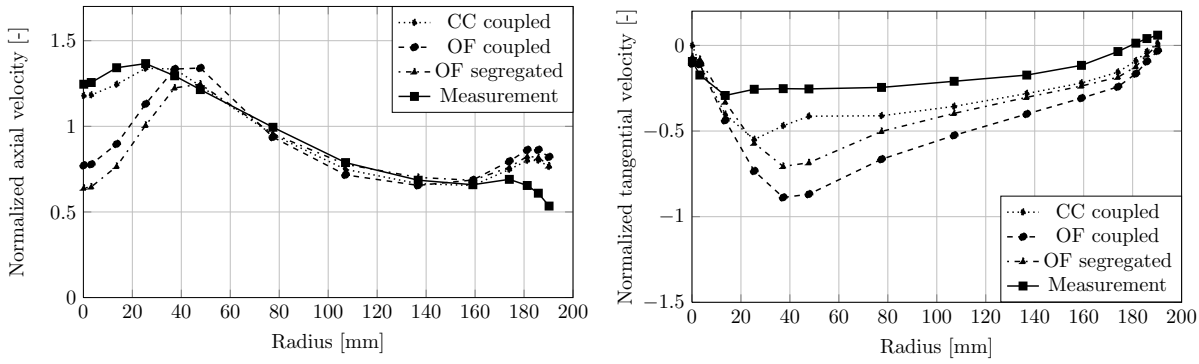

(a) Axial velocity (b) Tangential velocity

Figure 9: Normalized axial and tangential velocity at bottom slice in transient BEP operation.

3.4. Open issues

An open issue is the discrepancy of the tangential velocity evaluated by the LDA measurements and CFD simulations, especially at BEP conditions. All the numerically predicted tangential-velocities are far away from the experimental results. At the top slice, the experimental results show that the tangential velocity is approximately constant along the radius. As there are no flow guiding devices between the runner blade trailing edge and the evaluation planes, the flow in-between should more or less follow the free vortex law, where the product of the tangential velocity and the radius is a constant. Therefore, the distribution of the tangential velocity predicted by CFD seems qualitatively correct. Questionable is the development of the tangential velocity of the measurement from the top to the bottom plane. The tangential velocity peaks in the top plane at a radius of approximately 16 mm, while further down stream at the bottom plane is the maximum velocity close the zero radius. Never the less the area involved is rather small. In order to analyze the described discrepancy, an additional cut plane has been placed close to the runner trailing edge, as shown in figure 7. Figure 10 compares the numerical results of the coupled OpenFOAM solver applying the frozen rotor approach to the experimental results at the three evaluation planes. The tangential velocity evaluated at the plane closest to the runner trailing edge is approximately identical to that at the other evaluation planes.

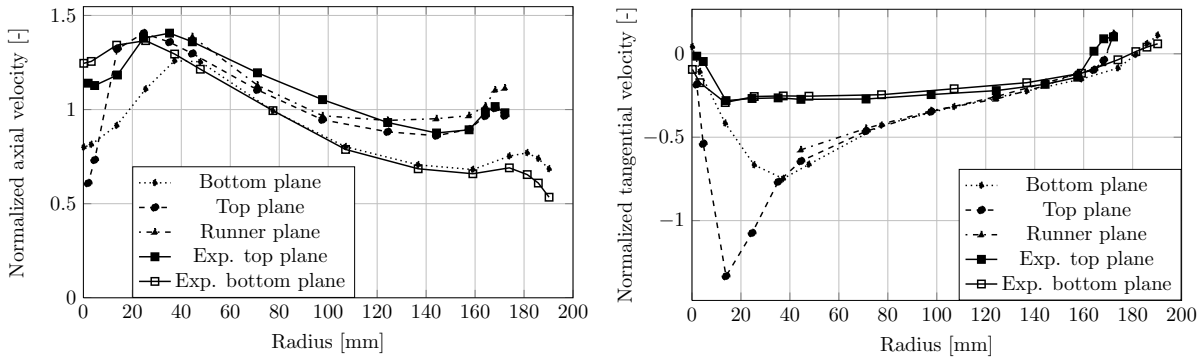

(a) Axial velocity (b) Tangential velocity

Figure 10: Normalized axial and tangential velocity at different cut plane positions at BEP operating conditions applying the steady-state coupled OpenFOAM solver.

Another open issue is that the integration of the measured axial velocity at PL conditions (figure 13a and 14a) does not well agree with the given volume flow rate. Below a radius of approximately 130 mm the measured axial velocity is negative and larger compared to the simulation and above it is smaller, which results in a overall lower volume flow rate compared to the simulation and therefore also the given data by the Francis-99 workshop [13].

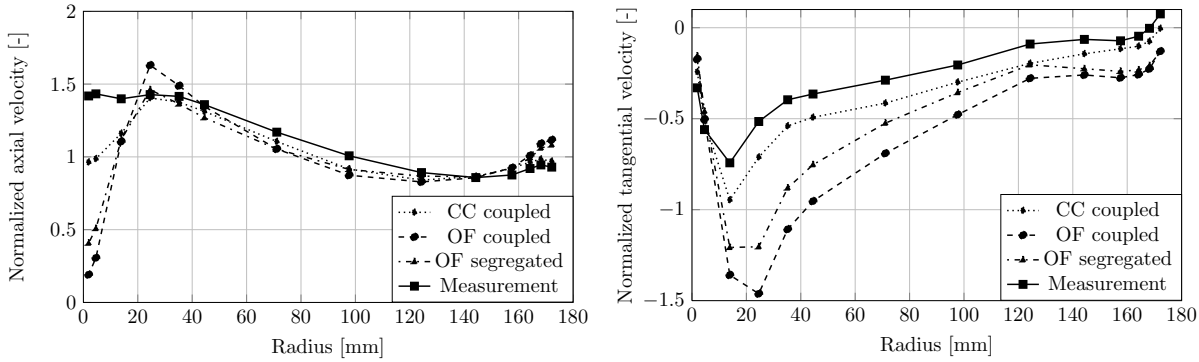

(a) Axial velocity (b) Tangential velocity

Figure 11: Normalized axial and tangential velocity at top slice in transient HL operation.

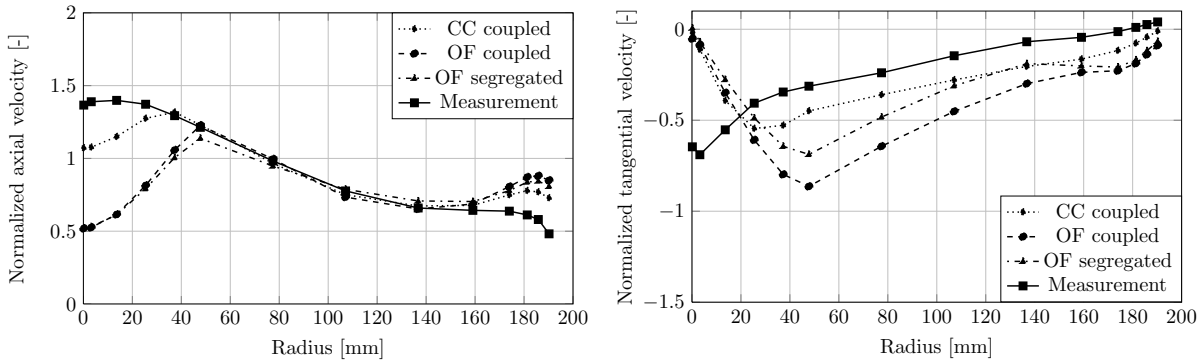

(a) Axial velocity (b) Tangential velocity

Figure 12: Normalized axial and tangential velocity at bottom slice in transient HL operation.

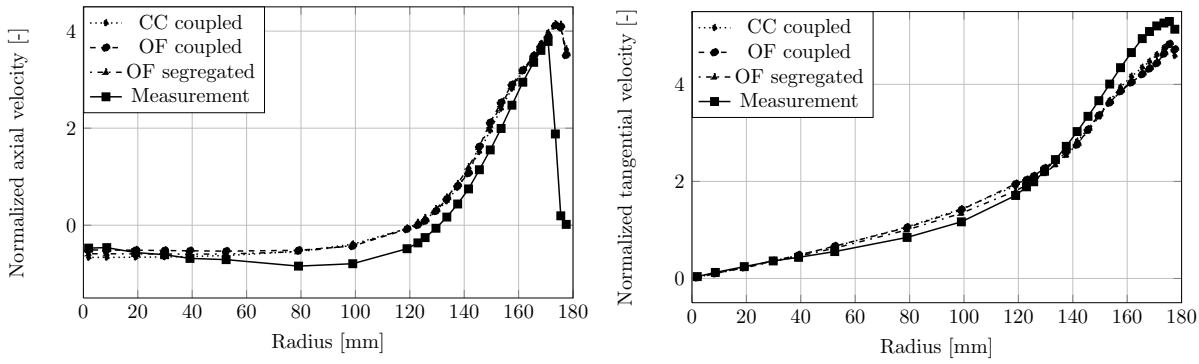

(a) Axial velocity (b) Tangential velocity

Figure 13: Normalized axial and tangential velocity at top slice in transient PL operation.

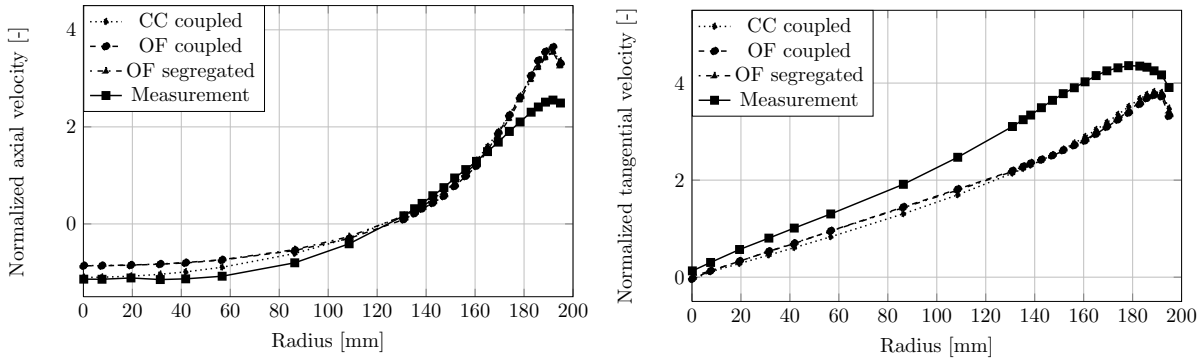

(a) Axial velocity (b) Tangential velocity

Figure 14: Normalized axial and tangential velocity at bottom slice in transient PL operation.

4. Conclusion

Steady-state as well as transient CFD computations of a 360 degrees high-head Francis-turbine model have been performed. Using a coupled approach for the pressure-velocity-coupling, a speed up of the steady-state and transient computational times of 4 to 5 and 1.5, respectively,

has been achieved. The developed coupled solver based on the framework of OpenFOAM, allows to predict the overall efficiency accurately compared to measurements and a reference commercial code. In general, the CFD codes overestimated the efficiency, because the simulation domain does not consider the rotor side spaces and the hereby associated losses. The steady-state frozen rotor results are in a surprisingly good agreement with the measurements, a reason for this could be the straight vortex rope especially in PL condition. Regarding the time dependent signals, the FFT shows a good comparison of the data with all three solvers in all operating points. The dominant frequencies are the blade passings and their multiples. The comparisons with the LDA-measurements are showing that the numerical prediction of the tangential velocity downstream of the runner trailing does not match with the measured velocity. The distribution of the measured velocities are questionable.

References

[1] NTNU and LTU *Francis-99 workshop* http://www.ltu.se/research/subjects/Stromningslara/Konferenser/Francis-99?l=en accessed august 2014
[2] Biesinger T, Cornelius C, Rube C, Braune A, Campregher R, Godin P G, Schmid G and Zori L 2010 Unsteady CFD methods in a commercial solver for turbomachinery applications *ASME Conference Proceedings* **2010** 44021
[3] Biesinger T, Cornelius C, Nuernberger D and Rube C 2012 Speed line computation of a transonic compressor stage with unsteady cfd methods *ASME Turbo Expo* **2012** 68029
[4] Mangani L, Buchmayr M and Darwish M 2014 Development of a novel fully coupled solver in openfoam: Steady state incompressible turbulent flows *Numerical Heat Transfer, Part B: Fundamentals* **66** p 1-20
[5] Patankar S 1980 *Numerical Heat Transfer and Fluid Flow* (Hemisphere Publishing, Washigton)
[6] Widmer C, Staubli T and Ledergerber N 2011 Unstable characteristics and rotating stall in turbine brake operation of pump-turbines *Journal of Fluids Engineering* **133** 041101
[7] Yan J P, Seidel U and Koutnik J 2012 Numerical simulation of hydrodynamics in a pump-turbine at off-design operating conditions in turbine mode *26th IAHR Symposium on Hydraulic Machinery and Systems* **15** 032041
[8] Feng J J, Li W F, Wu H, Lu J L, Liao W L and Luo X Q 2014 Investigation on pressure fluctuation in a francis turbine with improvement measures *27th IAHR Symposium on Hydraulic Machinery and Systems* **2014** 2.2.1
[9] Tamura Y, Tani K and Okamoto N 2014 Experimental and numerical investigation of unsteady behavior of cavitating vortices in draft tube of low specific speed francis turbine *27th IAHR Symposium on Hydraulic Machinery and Systems* **2014** 2.2.6
[10] Heo M W, Kim K Y, Ma S B, Yoo I S, Choi W C, Kim J H and Choi Y S 2014 Parametric performance evaluation of a hydraulic centrifugal pump *27th IAHR Symposium on Hydraulic Machinery and Systems* **2014** 3.1.6
[11] Guo P C, Guo D M, Sun L G and Luo X Q 2014 Numerical investigation of different volutes in a low specific speed centrifugal pump *27th IAHR Symposium on Hydraulic Machinery and Systems* **2014** 3.1.7
[12] Trivedi C, Cervantes M J, Gandhi B K and Dahlhaug O G 2013 Experimental and numerical studies for a high head francis turbine at several operating points *Journal of Fluids Engineering* **135(11)** 111102
[13] NTNU and LTU *Francis-99 test case* http://www.ltu.se/research/subjects/Stromningslara/Konferenser/Francis-99/Test-Case-1.111520?l=en accessed august 2014
[14] Staubli T, Loetscher B and Cimmino D 2005 Integrale laufrad- simulationen von hydromaschinen Tech. rep. FHZ-HTA
[15] Amoser M 1995 *Stroemungsfelder und Radialkraefte in Labyrinthdichtungen hydraulischer Stroemungsmaschinen* Ph.D. thesis ETH Zuerich
[16] OpenCFD 2014 *OpenFOAM User Guide* OpenCFD Limited
[17] Mangani L, Casartelli E and Mauri S 2011 Assessment of various turbulence models in a high pressure ratio centrifugal compressor with an object oriented CFD code *ASME Conference Proceedings* **2011** 54679